

Article

Modeling and Analysis of N-Branch Hybrid Switched Inductor and Capacitor Converter

Lei Yang ^{1,*} , Li Ma ¹, Xiaojie Li ¹, Liansong Xiong ^{2,3}, Xinghua Liu ¹ , Hui Cao ³  and Junkang Ni ⁴

¹ School of Electrical Engineering, Xi'an University of Technology, Xi'an 710048, China; 2180321214@stu.xaut.edu.cn (L.M.); 2201920045@stu.xaut.edu.cn (X.L.); liuxh@xaut.edu.cn (X.L.)

² School of Automation, Nanjing Institute of Technology, Nanjing 211167, China; xiongliansong@stu.xjtu.edu.cn

³ School of Electrical Engineering, Xi'an Jiaotong University, Xi'an 710049, China; huicao@mail.xjtu.edu.cn

⁴ School of Automation, Northwestern Polytechnical University, Xi'an 710072, China; junkangni@nwpu.edu.cn

* Correspondence: yanglei0930@xaut.edu.cn

Abstract: This paper proposes a family of N-Branch hybrid switched inductor and capacitor (SLC) converters. With the single circuit, the multi-level output voltage or current could be generated. The proposed converter is suitable both for the voltage source and the current source. The same LC network is reused for different LC branches. The proposed converter is controlled by the phase shift control method with a time domain multiplexing concept. The N level circuit is operated with the same frequency. One cycle period is divided into N small time cycles for each branch. The phase shift for each branch is $360^\circ/N$. The load voltage could be changed by modifying the duty cycle of the transistor. When the SLCs work in the resonant condition, the soft switching will be acquired. The power loss of transistors could be sharply reduced. In this paper, a 300 W SLC converter is constructed to verify the theoretical analysis and operation mechanism in the resonant condition and hard switching condition. With the experimental and simulated verification, the soft switching and the stable multi-level output voltage or current are achieved. The proposed SLC converter could be used for the multi-level voltage power supply system, such as the electric vehicle, the electric aircraft, autonomous underwater vehicles (AUVs) and a new energy generation system.

Keywords: hybrid switched inductor and capacitor (SLC) converter; time domain multiplexing concept; soft switching; multilevel output voltages



Citation: Yang, L.; Ma, L.; Li, X.; Xiong, L.; Liu, X.; Cao, H.; Ni, J. Modeling and Analysis of N-Branch Hybrid Switched Inductor and Capacitor Converter. *Electronics* **2021**, *10*, 891. <https://doi.org/10.3390/electronics10080891>

Academic Editor: Gabriel Garcera

Received: 18 March 2021

Accepted: 6 April 2021

Published: 8 April 2021

Publisher's Note: MDPI stays neutral with regard to jurisdictional claims in published maps and institutional affiliations.



Copyright: © 2021 by the authors. Licensee MDPI, Basel, Switzerland. This article is an open access article distributed under the terms and conditions of the Creative Commons Attribution (CC BY) license (<https://creativecommons.org/licenses/by/4.0/>).

1. Introduction

There are different kinds of DC–DC converters. The mostly popular one is the inductor-based converter. It includes a buck converter [1], boost converter, buck-boost converter, Cuk converter and so on. They could provide the stable voltage and current supply for different requirements. A switched capacitor (SC) converter has been widely used for renewable energy applications [2–4], implant medical devices [5–7], portable electric devices [8,9], data centers [10,11], and electric vehicles [12,13]. It has advantages such as ease of on-chip integration, being lightweight, and high-power density. The voltage conversion ratio of SC converters could be easily expanded through cascaded multiple SC cell topologies [14–18]. However, without the magnetic components, the current spikes will appear in the charge loop and discharge loop of a capacitor [19]. On the other hand, the input current of an SC converter will pulsate, leading to high current ripples and electromagnetic interference (EMI) noises [20,21]. The resonant switched-capacitor (RSC) converter is proposed for high-power applications. The small value inductor is injected into the charge loop or the discharge loop to reduce the spikes of the charging current and the discharging current [22,23]. What is more, the soft switching is achieved, which reduces the power loss of the transistors. However, in order to maintain the resonant condition, the load voltage is regulated in a very narrow range, which is hard for high-power applications.

The switched-inductor converter is proposed based on the switched-capacitor converter for the current source application [24–27]. It is widely used for PV system applications [28,29]. It provides an alternative power conversion method. This power conversion method is suitable for the current source and the current based load, such as LEDs. However, the application range of a switched-inductor converter is limited.

The inductor energy storage in the switched-inductor converter could reduce the current spikes. The capacitor energy storage in the switched-capacitor converter could reduce the ripples of the voltage. If the capacitor and inductor are used together, the quality of the converter could be highly improved, and the application range could then be largely extended. What is more, this kind of converter is suitable for both the current source and voltage source.

In a system, there are several required voltage levels for different applications [30–32]. The complex topology, such as buck-boost topology and modular multilevel topology, could provide the power supply for the different output voltage requirements. However, this method is high cost, and the power density is not high enough.

This paper proposes a family of N-Branch hybrid switched inductor and capacitor (SLC) converters; the combination of the capacitor energy storage and the inductor energy storage could bring an optimization of the traditional switched-capacitor converter and switched-inductor converter. It is both suitable for the current source and the voltage source. Moreover, it is good for the resistive load and the current based load. The pulsating input current and the input voltage ripples could be reduced with the proposed SLC converter. This converter provides multi-level voltage for different applications. It could be widely used for DC–DC power conversion.

The rest of the paper is organized as follows: the operation of the proposed SLC converter is shown in Section 2. Section 3 provides the theory analysis of the SLC converter. The theory verification is presented in Section 4. The conclusions and discussions are drawn in Section 5.

2. Operation Analysis of Proposed SLC Converter

The topology of the N-Branch SLC converter is shown in Figure 1. This SLC converter is a multi-level buck converter. Each branch circuit is divided and connected by a transistor. Based on the time domain multiplexing concept, the phase range of each branch is $\frac{360^\circ}{N}$. When the transistor is turned on in the Xth branch, the Xth branch is connected to the power source. In each branch, the load voltage could also be alternated by changing the duty-cycle of the transistor. A parallel connected LC network at the primary side of the SLC converter consists of the inductor L_R and the capacitor C_R . The pulsating input current could be reduced with the inductor L_R , and the input voltage ripples could be filtered by the capacitor C_R . In each branch circuit, there is a serial connected inductor and capacitor. If $L_R = L_1 = L_2 = L_3 = \dots = L_N$ and $C_R = C_1 = C_2 = C_3 = \dots = C_N$, the proposed SLC converter works in the resonant condition. The zero-voltage switching and the zero current switching is achieved. What is more, the SLC converter could work in the hard-switching condition to provide a wide regulated voltage range. This SLC converter could achieve the continuous load voltage and continuous load current with the duty-cycle control in each branch.

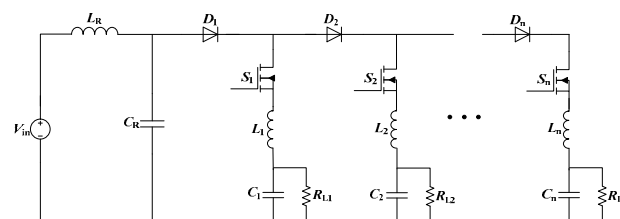


Figure 1. Topology of proposed N-Branch hybrid switched inductor and capacitor (SLC) converter.

The three-branch SLC converter is taken as an example to show the theory analysis and the operation method, which is shown in Figure 2. The timing waveforms of the

three-branch SLC converter are shown in Figure 3. It can be seen from Figure 3 that the phase shift of the transistor is set to 120° . The one switching cycle could be divided into three stages. The period of Stage 1 is from t_0 to t_2 . The period of Stage 2 is from t_2 to t_4 and the period of Stage 3 is from t_4 to t_6 .

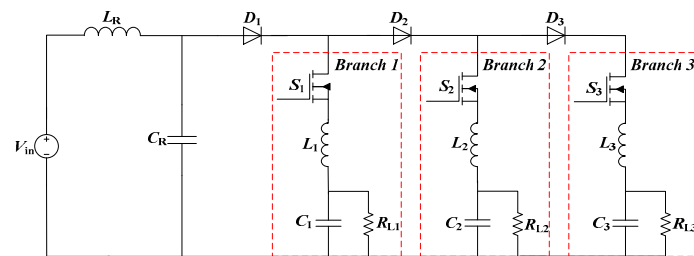


Figure 2. Three-branch SLC converter.

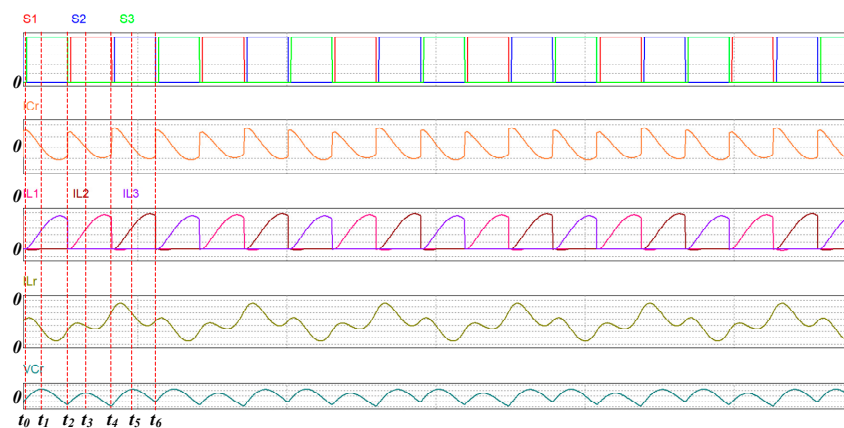


Figure 3. Timing waveforms of proposed SLC converter.

In Stage 1, S_1 is turned on while S_2 and S_3 are turned off; Branch 1 is connected to the power source. During the period ($t_0 \sim t_1$), the inductor L_R and capacitor C_R are charged by the power source at the same time. The current of inductor L_R and capacitor C_R is in the forward direction. During the same period, the power source transfers its energy to the inductor L_1 , capacitor C_1 and load resistor R_{L1} . During the period ($t_1 \sim t_2$), the direction of current capacitor C_R is changed. The power source, inductor L_R and capacitor C_R deliver their energy to inductor L_1 , capacitor C_1 and load resistor R_{L1} .

In Stage 2, S_2 is turned on while S_1 and S_3 are turned off; Branch 2 is connected to the power source. The charge and the discharge of inductor L_R and capacitor C_R are similar to Stage 1.

In Stage 3, S_3 is turned on while S_1 and S_2 are turned off; Branch 3 is connected to the power source. The charge and the discharge of inductor L_R and capacitor C_R are similar to Stage 1.

The relative operating states of the proposed SLC converter are shown in Figure 4. The charge of capacitor C_R and the discharge of capacitor C_R are kept balanced in one switching cycle. Moreover, the charge of inductor L_R and the discharge of inductor L_R are also kept balanced in one switching cycle. The inductor L_R and capacitor C_R build a LC compensation network. It could work in the resonant condition to transfer the maximum power level for the three LC branches.

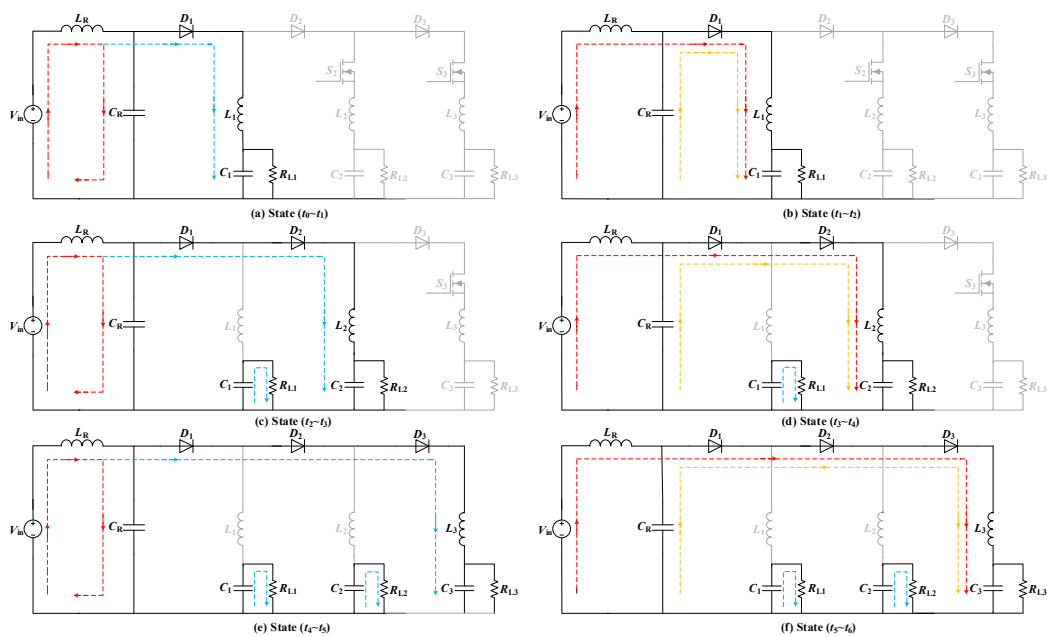


Figure 4. Operating states of proposed SLC converter.

The operation of the proposed SLC converter could be drawn in six states, as shown in Figure 4. During period ($t_0 \sim t_2$), when S_1 is on while S_2 and S_3 are off, there are States 1 and 2. As shown in Figure 4a, in State 1, the input current flows to the capacitor C_R and Branch 1. It can be seen from Figure 4b, in State 2, that the current of capacitor C_R and the input current both flow to Branch 1. During period ($t_2 \sim t_4$), when S_2 is on while S_1 and S_3 are off, there are States 3 and 4. As shown in Figure 4c, in State 3, the input current flows to the capacitor C_R and Branch 2. It can be seen from Figure 4d, in State 4, that the current of capacitor C_R and the input current both flow to Branch 2. During period ($t_4 \sim t_6$), when S_3 is on while S_1 and S_2 are off, there are States 5 and 6. As shown in Figure 4e, in State 5, the input current flows to the capacitor C_R and Branch 3. It can be seen from Figure 4f, in State 6, that the current of capacitor C_R and the input current both flow to Branch 3.

3. Theory Analysis of Proposed SLC Converter

For easy understanding, in the calculation, the internal resistance of the power source and diodes is ignored. What is more, the voltages of the diodes are also neglected. For the effectual regulation of the load voltage, the duty-cycle of each branch should be set to less than $\frac{1}{3}$.

The resonant frequency of the primary compensation network could be written as:

$$f_s = \frac{1}{2\pi\sqrt{L_r C_r}} \tag{1}$$

where L_r is the inductance of inductor L_R , and C_r is the capacitance of capacitor C_R .

When S_1 is turned on while S_2 and S_3 are turned off, Branch 1 is connected to the power source. In Stage 1, during the period ($t_0 \sim t_1$), as shown in Figure 4a, inductor L_R and C_R are charged by the power source. At the same time, the power delivers its energy to Branch 1. Based on the KVL principle, the following expressions are obtained:

$$L_r \frac{di_{Lr}(t)}{dt} = V_{in}(t) - V_{C1}(t) - V_{L1}(t) \tag{2}$$

$$i_{in}(t) = C_r \frac{dV_{Cr}(t)}{dt} + i_{in1}(t) \tag{3}$$

$$V_{Cr}(t) = V_{C1}(t) + V_{L1}(t) = V_{in} - V_{Lr}(t) \tag{4}$$

where $i_{Lr}(t)$ is the current of the inductor L_R , $V_{in}(t)$ is the input voltage, $V_{C1}(t)$ is the voltage of capacitor C_1 , $V_{L1}(t)$ is the voltage of inductor L_1 , $i_{in}(t)$ is the input current, C_r is the capacitance of capacitor C_R , $V_{Cr}(t)$ is the voltage of capacitor C_R , and $i_{in1}(t)$ is the input current of Branch 1.

From Figure 3, the boundary condition is:

$$i_{Cr}(t_1) = 0 \quad (5)$$

During the period ($t_1 \sim t_2$), as shown in Figure 4b, the power source, inductor L_R , and capacitor C_R deliver their energy to Branch 1 at the same time.

The following equations could be obtained:

$$i_{in1}(t) = C_r \frac{dV_{Cr}(t)}{dt} + i_{in}(t) \quad (6)$$

$$V_{Cr}(t) = V_{in}(t) + V_{Lr}(t) \quad (7)$$

When S_2 is turned on while S_1 and S_3 are turned off, Branch 2 is connected to the power source. In Stage 2, during the period ($t_2 \sim t_3$), as shown in Figure 4c, inductor L_R and C_R are charged by the power source. At the same time, the power delivers its energy to Branch 2. Based on the KVL principle, the following expression is obtained:

$$L_r \frac{di_{Lr}(t)}{dt} = V_{in}(t) - V_{C2}(t) - V_{L2}(t) \quad (8)$$

where $V_{C2}(t)$ is the voltage of capacitor C_2 , and $V_{L2}(t)$ is the voltage of inductor L_2 ;

$$V_{Cr}(t) = V_{in}(t) - V_{Lr}(t) \quad (9)$$

$$i_{in}(t) = C_r \frac{dV_{Cr}(t)}{dt} + i_{in2}(t) \quad (10)$$

where $i_{in2}(t)$ is the input current of Branch 2.

It can be seen from Figure 3 that the boundary condition is:

$$i_{Cr}(t_3) = 0 \quad (11)$$

During the period ($t_3 \sim t_4$), as shown in Figure 4d, the power source, inductor L_R , and capacitor C_R deliver their energy to Branch 2.

The following equations could be obtained:

$$i_{in2}(t) = C_r \frac{dV_{Cr}(t)}{dt} + i_{in}(t) \quad (12)$$

$$V_{Cr}(t) = V_{in}(t) + V_{Lr}(t) \quad (13)$$

It can be seen from Figure 3 that the boundary condition is:

$$i_{Cr}(t_4) = 0 \quad (14)$$

When S_3 is turned on while S_1 and S_2 are turned off, Branch 3 is connected to the power source. In Stage 3, during the period ($t_4 \sim t_5$), as shown in Figure 4e, inductor L_R and C_R are charged by the power source. At the same time, the power delivers its energy to Branch 3. Based on the KVL principle, the following expression is obtained:

$$L_r \frac{di_{Lr}(t)}{dt} = V_{in}(t) - V_{C3}(t) - V_{L3}(t) \quad (15)$$

where $V_{C3}(t)$ is the voltage of capacitor C_3 , and $V_{L3}(t)$ is the voltage of inductor L_3 ;

$$V_{Cr}(t) = V_{in} - V_{Lr}(t) \tag{16}$$

$$i_{in}(t) = C_r \frac{dV_{Cr}(t)}{dt} + i_{in3}(t) \tag{17}$$

where $i_{in3}(t)$ is the input current of Branch 3.

It can be seen from Figure 3 that the boundary condition is:

$$i_{Cr}(t_5) = 0 \tag{18}$$

During the period ($t_5 \sim t_6$), as shown in Figure 4f, the power source, inductor L_R , and capacitor C_R deliver their energy to Branch 3.

The following equations could be obtained:

$$i_{in3}(t) = C_r \frac{dV_{Cr}(t)}{dt} + i_{in}(t) \tag{19}$$

$$V_{Cr}(t) = V_{in}(t) + V_{Lr}(t) \tag{20}$$

It can be seen from Figure 3 that the boundary condition is:

$$i_{Cr}(t_6) = 0 \tag{21}$$

In one switching cycle, the charge and discharge of inductor L_R and capacitor C_R are kept balanced. Based on the aforementioned discussion and calculation, it can be seen from Figure 3 that the total charge of capacitor C_R and total discharge of capacitor C_R could be respectively derived as:

$$Q_{Cr(\text{charge})} = \int_{t_0}^{t_1} C_r \frac{dV_{Cr}(t)}{dt} dt + \int_{t_2}^{t_3} C_r \frac{dV_{Cr}(t)}{dt} dt + \int_{t_4}^{t_5} C_r \frac{dV_{Cr}(t)}{dt} dt \tag{22}$$

$$Q_{Cr(\text{discharge})} = \left[\int_{t_1}^{t_2} C_r \frac{dV_{Cr}(t)}{dt} dt + \int_{t_3}^{t_4} C_r \frac{dV_{Cr}(t)}{dt} dt + \int_{t_5}^{t_6} C_r \frac{dV_{Cr}(t)}{dt} dt \right] \tag{23}$$

In one switching cycle period, the charge balance of capacitor C_R could be written as:

$$Q_{Cr(\text{charge})} + Q_{Cr(\text{discharge})} = 0 \tag{24}$$

Substituting (22) and (23) into (24), the charge balance of capacitor C_R in one switching cycle of capacitor could be derived as:

$$\left[\int_{t_0}^{t_1} C_r \frac{dV_{Cr}(t)}{dt} dt + \int_{t_2}^{t_3} C_r \frac{dV_{Cr}(t)}{dt} dt + \int_{t_4}^{t_5} C_r \frac{dV_{Cr}(t)}{dt} dt \right] + \left[\int_{t_1}^{t_2} C_r \frac{dV_{Cr}(t)}{dt} dt + \int_{t_3}^{t_4} C_r \frac{dV_{Cr}(t)}{dt} dt + \int_{t_5}^{t_6} C_r \frac{dV_{Cr}(t)}{dt} dt \right] = 0 \tag{25}$$

During the period ($t_0 \sim t_2$), the following equation does always stand up.

$$V_{Cr}(t) = V_{o1}(t) + V_{L1}(t) \tag{26}$$

During the period ($t_2 \sim t_4$), the following equation does always stand up.

$$V_{Cr}(t) = V_{o2}(t) + V_{L2}(t) \tag{27}$$

During the period ($t_4 \sim t_6$), the following equation could be derived.

$$V_{Cr}(t) = V_{o2}(t) + V_{L3}(t) \tag{28}$$

As a result, the average load voltages V_{o1} , V_{o2} and V_{o3} in one switching cycle could be expressed as:

$$V_{o1} = \frac{3 \int_{t_0}^{t_2} [V_{Cr}(t) - V_{L1}(t)] dt}{T_s} \tag{29}$$

$$V_{o2} = \frac{3 \int_{t_2}^{t_4} [V_{Cr}(t) - V_{L2}(t)] dt}{T_s} \quad (30)$$

$$V_{o3} = \frac{3 \int_{t_4}^{t_6} [V_{Cr}(t) - V_{L3}(t)] dt}{T_s} \quad (31)$$

In this paper, D_1 is set as the duty cycle of S_1 , D_2 is set as the duty cycle of S_2 and D_3 is set as the duty cycle of S_3 . The duty cycle could be changed to achieve the different load voltage.

If $D_1 \leq \frac{1}{3}$, $D_2 \leq \frac{1}{3}$, and $D_3 \leq \frac{1}{3}$, the average load voltages V_{o1} , V_{o2} , and V_{o3} , in one switching cycle, could be expressed as:

$$V_{o1} = \frac{3 \int_0^{D_1 T_s} [V_{Cr}(t) - V_{L1}(t)] dt}{T_s} \quad (32)$$

$$V_{o2} = \frac{3 \int_0^{D_2 T_s} [V_{Cr}(t) - V_{L2}(t)] dt}{T_s} \quad (33)$$

$$V_{o3} = \frac{3 \int_0^{D_3 T_s} [V_{Cr}(t) - V_{L3}(t)] dt}{T_s} \quad (34)$$

4. Experimental and Simulated Verification

In order to verify the performance and mechanism of the SLC converter, a 300 W power level SLC converter is constructed in this paper. The experimental SLC converter is shown in Figure 5. The power circuit and control unit are integrated in the same PCB board. The performance of the proposed SLC converter is respectively tested in the resonant condition and the normal condition. The parameters of the proposed SLC converter are shown in Table 1.

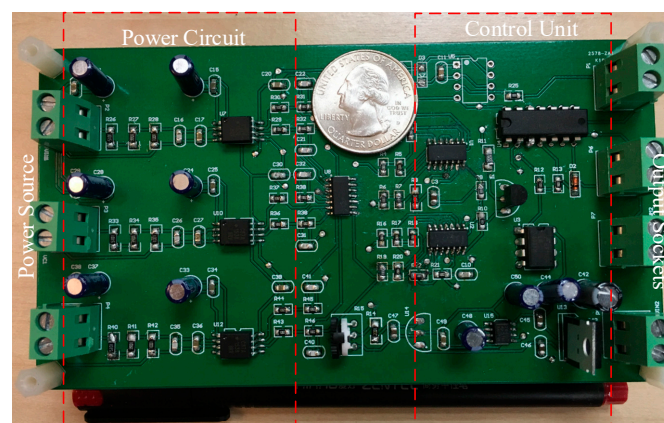


Figure 5. Experimental SLC converter with control unit.

Table 1. Circuit parameters.

Parameters	Value
L_r	5 μ H/20 μ H
C_r	10 μ F
L_1, L_2, L_3	5 μ H
C_1, C_2, C_3	10 μ F
S_1, S_2, S_3, S_4	N channel MOSFET, IRF640NPBF, $V_{dss} = 200$ V, $I_d = 18$ A, 150 m Ω @ 11 A, 10 V, 150 W

Table 1. Cont.

Parameters	Value
D_1, D_2, D_3	Fast Recovery Diode, VS-20CTH03STRL-M3, $V_r = 300$ V, $I_o = 10$ A, $V_f = 1.25$ V@10 A, $t_{rr} = 35$ ns.
Input voltage	50 V and 100 V
Switching frequency	22.51 kHz/100 kHz
$R_{L1} = R_{L2} = R_{L3}$	0~1000 Ω

4.1. Case 1: Charge Balance Validation

As shown in Figure 6, if the switching frequency is set to 22.51 kHz, the proposed SLC converter works in the resonant condition. It can be seen that the waveforms of the input current and the currents of Branch 1, Branch 2 and Branch 3 meet the theory analysis. The smoothly input current is achieved. The current spikes of the transistors are highly reduced with the LC network in each branch. As shown in Figure 6, in one switching cycle, the summation of the charge of capacitor C_R and the discharge of capacitor C_R equal zero. This is the same for the inductor L_R . As a result, the charge balance of inductor L_R and capacitor C_R in one switching cycle is verified.

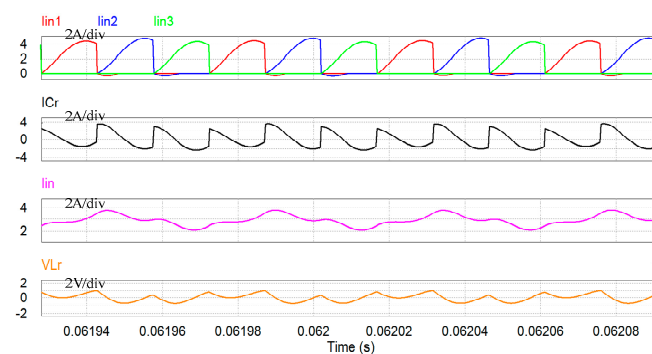


Figure 6. Operating waveforms of currents of proposed three-branch SLC converter.

4.2. Case 2: Soft Switching Validation

In the resonant condition, the ZVS and ZCS are achieved with the proposed SLC converter, as shown in Figure 7. When the switching frequency is set to 100 kHz (the duty cycle of S_1 is 0.2, the duty cycle of S_2 is 0.1 and the duty cycle of S_3 is 0.33), it can be seen from Figure 8 that the different voltages (33.19 V, 17.00 V and 41.23 V) are achieved by changing the duty-cycle of the transistor in each branch with the load resistance 50 Ω . The load voltage ripple factors of the three branches are respectively 0.80%, 0.85% and 0.69%. As a result, with a suitable regulation, the load voltage could be steadily controlled with good performance.

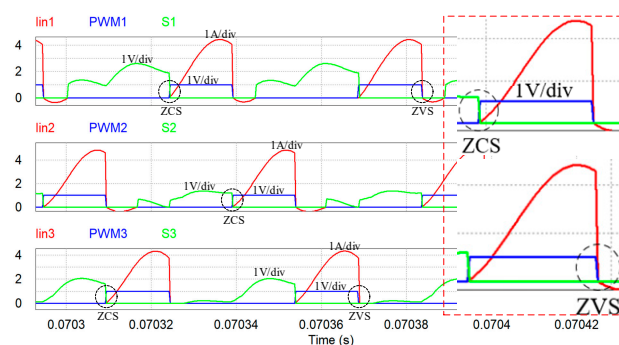


Figure 7. Soft switching of proposed three-branch SLC converter (voltage source).

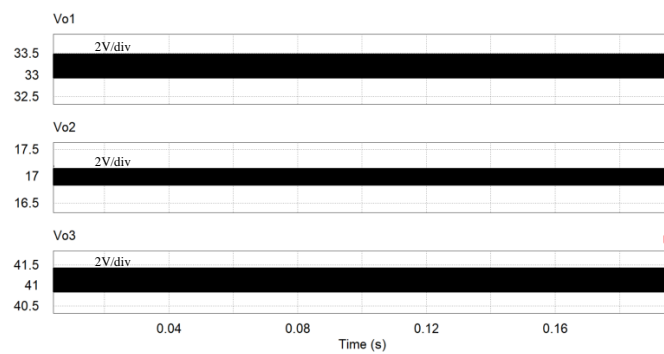


Figure 8. Operating waveforms of load voltages with frequency 100 kHz (voltage source).

4.3. Case 3: Current Source Validation

To demonstrate the suitable application for the current source, the simulation is conducted with a 5 A current source. When the proposed SLC converter works in the resonant condition, as can be seen in Figure 9, the input current is kept stable with very small ripples. The input currents of Branch 1, Branch 2 and Branch 3 are regulated smoothly without high spikes. The current spikes of the transistors are highly reduced with the LC network in each branch. In the resonant condition, as shown in Figure 10, the transistor could be turned on in the ZCS condition and turned off in the ZVS condition. The soft switching is achieved with the proposed SLC converter. It can be seen from Figure 11 that the load currents of the three branches are measured with the switching frequency of 100 kHz. When the switching frequency is set to 100 kHz (the duty-cycle of S_1 is 0.2, the duty cycle of S_2 is 0.1 and the duty cycle of S_3 is 0.33), as shown in Figure 11, the different currents (1.80 A, 0.93 A and 2.27 A) are achieved by changing the duty-cycle of the transistor in each branch with the load resistance 50 Ω . The load current ripple factors of the three branches are 0.79%, 0.87% and 0.69%. As a result, with a suitable regulation, the load current could be steadily controlled with good performance. The simulation results have a good match to the theory analysis.

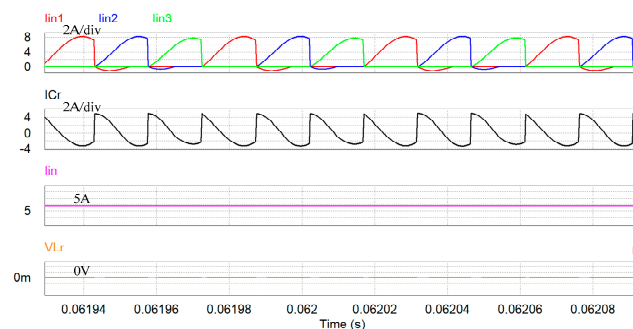


Figure 9. Operating waveforms of currents of proposed three-branch SLC converter (current source).

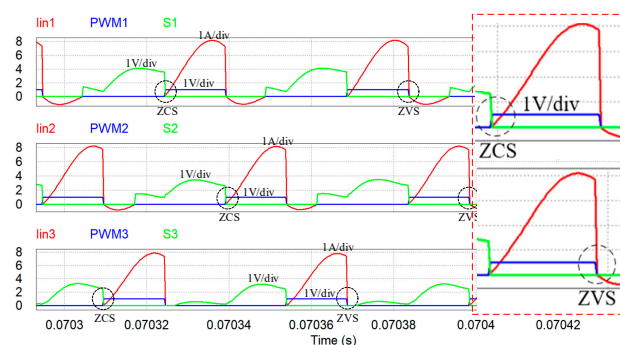


Figure 10. Soft switching of proposed three-branch SLC converter (current source).

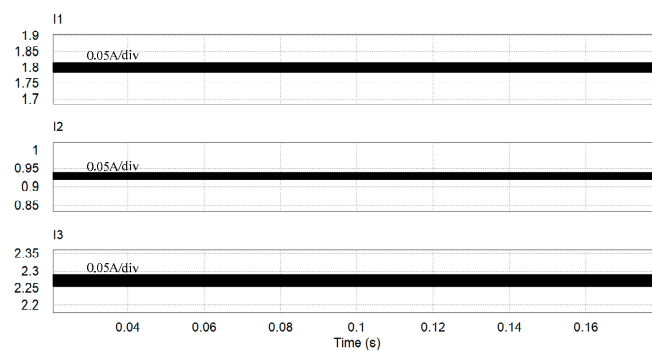


Figure 11. Operating waveforms of load voltages with frequency 100 kHz (current source).

As shown in Figure 12, with the same duty cycle of the transistors, the constant currents of the different branches will be achieved with different load power levels. It can be seen from Figure 12 that the input current source is set to 1 A, and the duty cycle of the three transistors of the three branches is set to 0.33. If the load resistors of Branch 1, Branch 2 and Branch 3 are set to 20 Ω , 50 Ω and 100 Ω , the load currents of the three branches are, respectively, 0.34 A, 0.33 A and 0.33 A. The constant current does not depend on the load power level. This is a specific feature of the SLC converter.

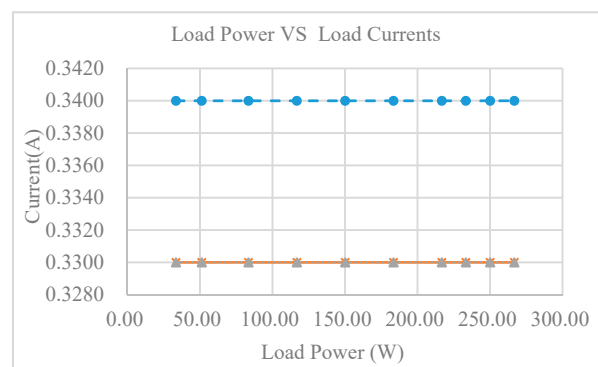


Figure 12. Operating waveforms of load currents with 1 A current source.

4.4. Case 4: Comparison of Voltage Source and Current Source

The operating waveforms of public capacitor C_R and inductor L_R are also measured in this paper. It can be seen from Figure 13 that, with the rising switching frequency, the voltage ripples of capacitor C_R and the current ripples of inductor L_R will be reduced. When the SLC converter works in the resonant condition (22.51 kHz), the sinusoidal voltage and sinusoidal current will be achieved with low EMI noise, as shown in Figure 13. With the 5 A current source, the value of the current ripples of inductor L_R is almost zero. With the 100 V input voltage source, the maximum peak to peak voltage ripple of capacitor C_R and the maximum peak to peak current ripple of inductor L_R are respectively 3 V and 2 A.

The V_o vs. duty-cycle and I_o vs. duty-cycle of Branch 1 are respectively measured with the voltage source and the current source. The duty-cycle of S_2 and duty-cycle S_3 are both set to 0.31. The results are shown in Figure 14. The switching frequency is 100 kHz. It can be seen from Figure 14 that the output voltage and output current will both increase with the rising of the duty-cycle for the voltage source and the current source.

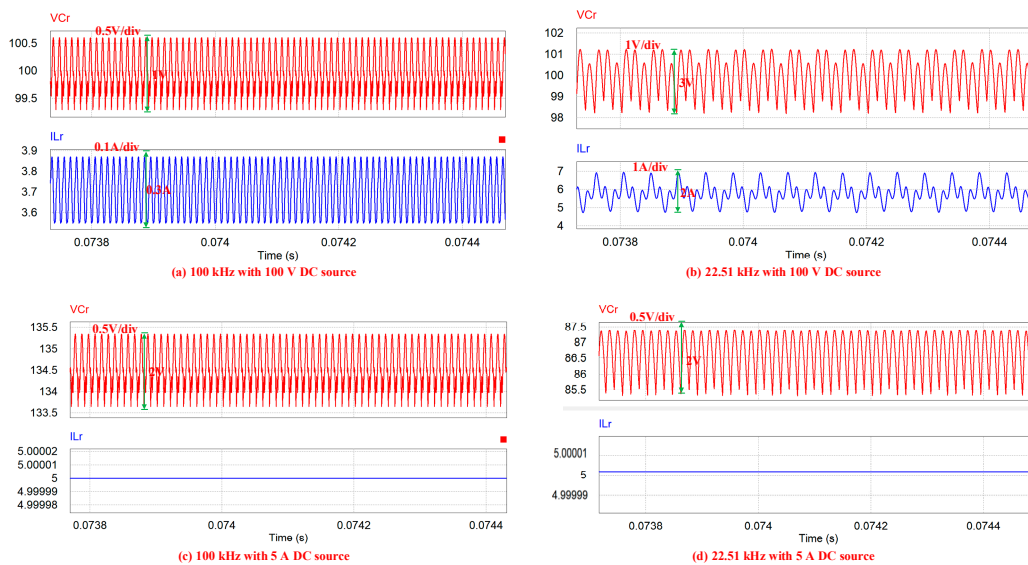
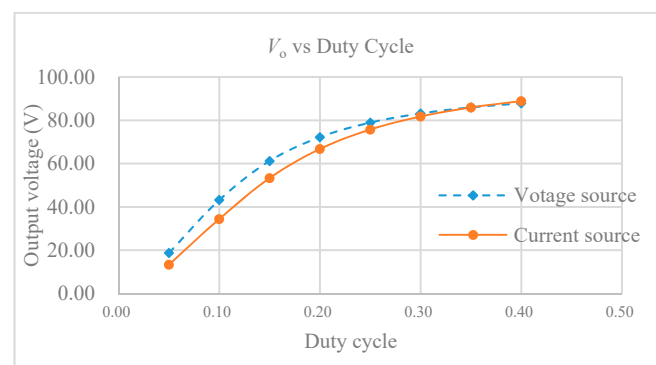
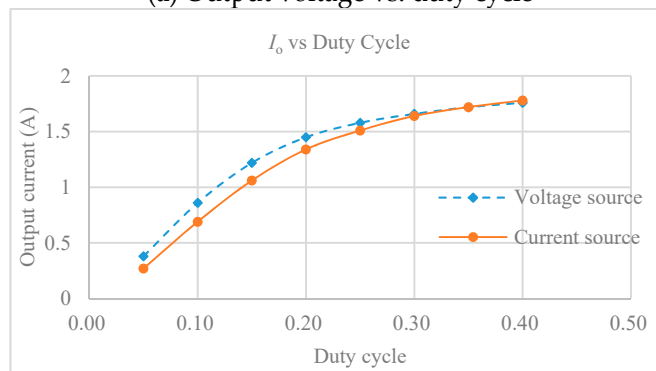


Figure 13. Operating waveforms of capacitor C_R and inductor and inductor L_R .



(a) Output voltage vs. duty cycle



(b) Output current vs. duty cycle

Figure 14. V_o vs. duty-cycle and I_o vs. duty-cycle of Branch 1.

4.5. Case 5: Experimental Validation

To verify the theory analysis, experiments were conducted in the laboratory. A 300 W power level three-branch SLC converter was built and tested as the experimental object. The voltage source was adapted in the experiments. The input voltages were respectively set to 50 V and 100 V. The duty-cycle of S_1 in branch 1 was set to 0.2. The switching frequency of all transistors was set to 100 kHz. As shown in Figure 15, the stable load voltage and current were achieved with 100 V input voltage. The input voltage of the three-branch SLC converter is continuous and smooth without high spikes. What is more,

when the input voltage was changed to 50 V and the duty-cycle was set to 0.3 for all transistors of the SLC converter, the tested waveforms of the load voltages of the three branches were obtained and are shown in Figure 16. It can be seen from Figure 16 that the output voltages of the three branches are similar. The amplitude is about 48 V. As a result, the multilevel output voltages could be acquired with the single SLC topology. The good performance of the SLC converter is verified with the simple topology.

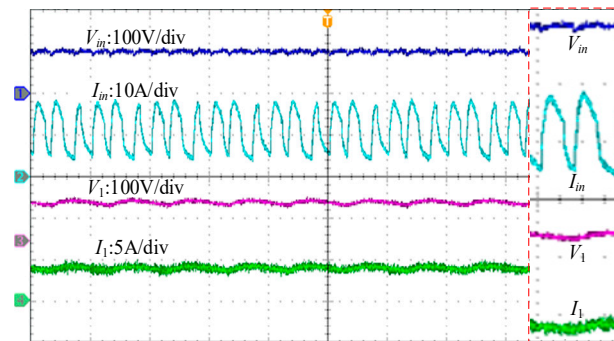


Figure 15. Load voltage and load current of Branch 1 with 100 V input voltage.

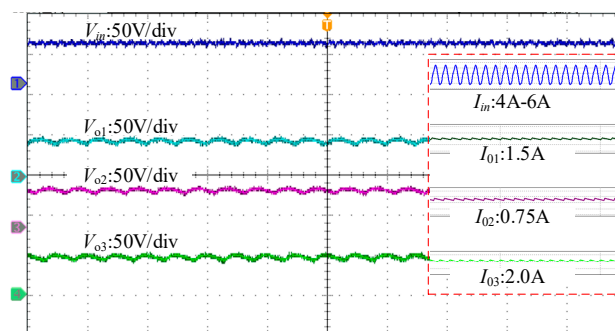


Figure 16. Load voltages and load currents of three-branch SLC converter with 50 V input voltage.

4.6. Case 6: Efficiency Analysis

The efficiency of the proposed SLC converter is respectively tested with the voltage source and the current source. The high efficiency is achieved with the proposed SLC converter. The tested results are respectively shown in Figures 17 and 18. The switching frequency is set to 100 kHz in the experiments. As shown in Figure 17, with the voltage source, the highest efficiency of the proposed SLC converter is 98.62% at the load power of 70 W. It can be seen from Figure 18 that, with the current source, the highest tested efficiency of the proposed SLC converter is 98.49% at the load power 270 W. The conclusion could be derived from the measured data, as shown in Figures 17 and 18, that, with the voltage source, the efficiency of the proposed SLC converter will decrease with the increasing of the load power; however, with the current source, the efficiency of the proposed SLC converter will climb with the increasing of the load power.

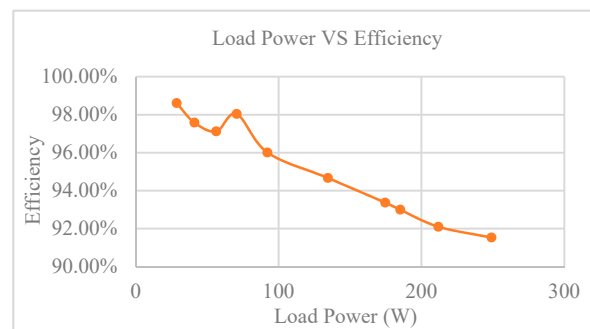


Figure 17. Measured efficiency of proposed SLC converter with the voltage source.

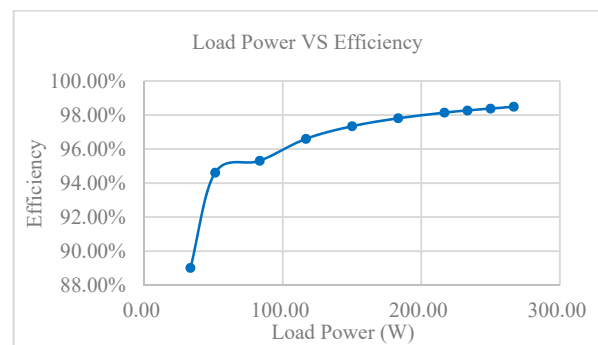


Figure 18. Measured efficiency of proposed SLC converter with the current source.

5. Conclusions and Discussion

An innovative N-Branch SLC converter is proposed in this paper. The LC resonant network is used for the power transfer unit. When the proposed SLC converter works in the resonant condition, the ZVS and ZCS are achieved. The proposed SLC converter is suitable for both the voltage source and the current source. The multi-level voltage or current could be realized by extending the branches and sharing the same primary LC network. The time domain multiplexing concept is used in this paper by dividing the one switching cycle phase to $\frac{360^\circ}{N}$. The PWM control method is adapted to get the required load voltage or current. Moreover, the continuous input current could be achieved with the voltage source. The simulated and experimental results show that the stable multi-level load voltage or current could be realized with the proposed SLC converter. The high efficiency of the proposed SLC converter is achieved with the simple topology. This SLC converter extends the application range of the converter for resistive loads and current based loads.

Author Contributions: L.Y. initiated the idea and designed the converter. L.M. and X.L. (Xiaojie Li) did the simulations and drafted the article. L.X., X.L. (Xinghua Liu), H.C. and J.N. initiated the conceptualization. L.M. did the formal analysis. All authors contributed towards extensive revisions of the article. All authors have read and agreed to the published version of the manuscript.

Funding: This work was supported by the China Postdoctoral Science Foundation under grant no.2018M643700, Scientific Research Project of Education Department of Shaanxi Province under grant no.18JS080, Postdoctoral Research Program of Shaanxi Province under grant no. 2018BSHY-DZZ28, Basic Research Project of Natural Science of Shaanxi Province under grant no.2020JQ-632, and Basic Research Project of Natural Science of Shaanxi Province under grant no.2020JQ-623.

Conflicts of Interest: The authors declare no conflict of interest. The funders had no role in the design of the study; in the collection, analyses, or interpretation of data; in the writing of the manuscript, or in the decision to publish the results.

References

1. Das, S.; Salim, K.M.; Chowdhury, D. A novel variable width PWM switching based buck converter to control power factor correction phenomenon for an efficacious grid integrated electric vehicle battery charger. In Proceedings of the TENCON 2017—2017 IEEE Region 10 Conference, Penang, Malaysia, 5 November 2017; pp. 262–267.
2. Uno, M.; Sugiyama, K. Switched Capacitor Converter Based Multiport Converter Integrating Bidirectional PWM and Series-Resonant Converters for Standalone Photovoltaic Systems. *IEEE Trans. Power Electron.* **2019**, *34*, 1394–1406. [\[CrossRef\]](#)
3. Li, K.; Yin, Z.; Yang, Y.; Wang, Y.Y.H.; Blaabjerg, F. A switched-capacitor based high conversion ratio converter for renewable energy applications: Principle and generation. In Proceedings of the 2017 IEEE Energy Conversion Congress and Exposition (ECCE), Cincinnati, OH, USA, 1–5 October 2017; pp. 3440–3556.
4. Parastar, A.; Seok, J.-K. High-Gain Resonant Switched-Capacitor Cell-Based DC/DC Converter for Offshore Wind Energy Systems. *IEEE Trans. Power Electron.* **2015**, *30*, 644–656. [\[CrossRef\]](#)
5. Lee, H.; Jang, E.; Saif, H.; Lee, Y.; Kim, M.; Khan, M.B.; Lee, Y. A Sub-nW Fully Integrated Switched-Capacitor Energy Harvester for Implantable Applications. In Proceedings of the ESSCIRC 2018-IEEE 44th European Solid State Circuits Conference (ESSCIRC), Dresden, Germany, 3–6 September 2018; pp. 50–53.
6. Ballo, A.; Bottaro, M.; Grasso, A.D.; Palumbo, G.; Grasso, A.D. Regulated Charge Pumps: A Comparative Study by Means of Verilog-AMS. *Electronics* **2020**, *9*, 998. [\[CrossRef\]](#)
7. Ballo, A.; Bottaro, M.; Grasso, A. A Review of Power Management Integrated Circuits for Ultrasound-Based Energy Harvesting in Implantable Medical Devices. *Appl. Sci.* **2021**, *11*, 2487. [\[CrossRef\]](#)
8. Zhao, C.; Cochran, S.; Costinett, D.; Yang, S. Design and Evaluation of a Multilevel Switched Capacitor Rectifier for Wireless Fast Charging. In Proceedings of the 2019 IEEE Applied Power Electronics Conference and Exposition (APEC), Anaheim, CA, USA, 17–21 March 2019; pp. 833–840.
9. Kesarwani, K.; Sangwan, R.; Stauth, J.T. Resonant-Switched Capacitor Converters for Chip-Scale Power Delivery: Design and Implementation. *IEEE Trans. Power Electron.* **2015**, *30*, 6966–6977. [\[CrossRef\]](#)
10. Saggini, S.; Jiang, S.; Ursino, M.; Nan, C. A 99% Efficient Dual-Phase Resonant Switched-Capacitor-Buck Converter for 48 V Data Center Bus Conversions. In Proceedings of the 2019 IEEE Applied Power Electronics Conference and Exposition (APEC), Anaheim, CA, USA, 17–21 March 2019; pp. 482–487.
11. Li, Y.; Lyu, X.; Cao, D.; Jiang, S.; Nan, C. A 98.55% Efficiency Switched-Tank Converter for Data Center Application. *IEEE Trans. Ind. Appl.* **2018**, *54*, 6205–6222. [\[CrossRef\]](#)
12. Janabi, A.; Wang, B. Switched-Capacitor Voltage Boost Converter for Electric and Hybrid Electric Vehicle Drives. *IEEE Trans. Power Electron.* **2019**, *35*, 5615–5624. [\[CrossRef\]](#)
13. Zhang, Y.; Gao, Y.; Zhou, L.; Sumner, M. A Switched-Capacitor Bidirectional DC–DC Converter with Wide Voltage Gain Range for Electric Vehicles With Hybrid Energy Sources. *IEEE Trans. Power Electron.* **2018**, *33*, 9459–9469. [\[CrossRef\]](#)
14. Sato, Y.; Uno, M.; Nagata, H. Nonisolated Multiport Converters Based on Integration of PWM Converter and Phase-Shift-Switched Capacitor Converter. *IEEE Trans. Power Electron.* **2020**, *35*, 455–470. [\[CrossRef\]](#)
15. Ye, Z.; Lei, Y.; Pilawa-Podgurski, R.C.N. The Cascaded Resonant Converter: A Hybrid Switched-Capacitor Topology with High Power Density and Efficiency. *IEEE Trans. Power Electron.* **2020**, *35*, 4946–4958. [\[CrossRef\]](#)
16. Xie, W.; Li, S.; Smedley, K.M.; Wang, J.; Ji, Y.; Yu, J. A Family of Dual Resonant Switched-Capacitor Converter with Passive Regenerative Snubber. *IEEE Trans. Power Electron.* **2019**, *35*, 4891–4904. [\[CrossRef\]](#)
17. Ballo, A.; Grasso, A.D.; Palumbo, G.; Tanzawa, T. Linear distribution of capacitance in Dickson charge pumps to reduce rise time. *Int. J. Circuit Theory Appl.* **2020**, *48*, 555–566. [\[CrossRef\]](#)
18. Ballo, A.; Grasso, A.D.; Palumbo, G. Charge Pump Improvement for Energy Harvesting Applications by Node Pre-Charging. *IEEE Trans. Circuits Syst. II Express Briefs* **2020**, *67*, 3312–3316. [\[CrossRef\]](#)
19. Axelrod, B.; Berkovich, Y.; Ioinovici, A. Switched-Capacitor/Switched-Inductor Structures for Getting Transformerless Hybrid DC–DC PWM Converters. *IEEE Trans. Circuits Syst. I Regul. Pap.* **2008**, *55*, 687–696. [\[CrossRef\]](#)
20. Cao, D.; Peng, F.Z. Zero-Current-Switching Multilevel Modular Switched-Capacitor DC–DC Converter. In Proceedings of the 2009 IEEE Energy Conversion Congress and Exposition, San Jose, CA, USA, 20–24 September 2009; pp. 3516–3522.
21. Xiong, L.; Liu, X.; Zhao, C.; Zhuo, F. A Fast and Robust Real-Time Detection Algorithm of Decaying DC Transient and Harmonic Components in Three-Phase Systems. *IEEE Trans. Power Electron.* **2019**, *35*, 3332–3336. [\[CrossRef\]](#)
22. De Albuquerque, V.M.; Soares, G.M.; Alonso, J.M.; Almeida, P.S. A Simple Resonant Switched-Capacitor LED Driver Employed as a Fast Pulse-Based Transmitter for VLC Applications. *IEEE J. Emerg. Sel. Top. Power Electron.* **2021**, *9*, 111–122. [\[CrossRef\]](#)
23. Yang, X.; Zhang, Y.C.; Wen, P.; Liu, Y.; Zheng, T.Q.; Takaku, T.; Igarashi, S. Improved Phase Shift Control for SiC-MOSFET Based Resonant Switched-Capacitor Converter with Parasitics Consideration. *IEEE Trans. Ind. Appl.* **2020**, *56*, 3995–4006. [\[CrossRef\]](#)
24. Fardahar, S.M.; Sabahi, M. New Expandable Switched-Capacitor/Switched-Inductor High-Voltage Conversion Ratio Bidirectional DC–DC Converter. *IEEE Trans. Power Electron.* **2019**, *35*, 2480–2487. [\[CrossRef\]](#)
25. Zheng, Y.; Smedley, K.M. Analysis and Design of a Single-Switch High Step-Up Coupled-Inductor Boost Converter. *IEEE Trans. Power Electron.* **2019**, *35*, 535–545. [\[CrossRef\]](#)
26. Cheng, K.W.E.; Ye, Y. Duality approach to the study of switched-inductor power converters and its higher-order variations. *IET Power Electron.* **2015**, *8*, 489–496. [\[CrossRef\]](#)

27. Higa, H.; Sagawa, A.; Itoh, J.-I. Improvement of Light Load Efficiency for Buck-Boost DC-DC converter with ZVS using Switched Auxiliary Inductors. In Proceedings of the 2018 IEEE International Power Electronics and Application Conference and Exposition (PEAC), Shenzhen, China, 4–7 November 2018; pp. 1–6.
28. Maroti, P.K.; Ranjana, M.S.B.; Prabhakar, D.K. A novel high gain switched inductor multilevel buck-boost DC-DC converter for solar applications. In Proceedings of the 2014 IEEE 2nd International Conference on Electrical Energy Systems (ICEES), Chennai, India, 7–9 January 2014; pp. 152–156.
29. Singh, G.; Srivastava, S.; Lalwani, R.; Tewari, N.; Prabhakar, M. High Gain DC-DC Converter Based on Hybrid Switched-Inductor Topology for PV Application. In Proceedings of the 2019 IEEE International Conference on System, Computation, Automation and Networking (ICSCAN), Pondicherry, India, 29–30 March 2019; pp. 1–6.
30. Patro, S.K.; Shukla, A. Modular Directed Series Multilevel Converter for HVDC Applications. *IEEE Trans. Ind. Appl.* **2020**, *56*, 1618–1630. [[CrossRef](#)]
31. Jafari, M.; Jafarishiadeh, F.; Ghasemi, A.; Shojaeighadikolaie, A.; Saadatmand, S.; Ahmadi, R. New MMC-Based Multilevel Converter with Two-And-One Set of Arms and One Inductor. In Proceedings of the 2020 IEEE Power and Energy Conference at Illinois (PECI), Champaign, IL, USA, 27–28 February 2020; pp. 1–4.
32. Ajaykumar, T.; Patne, N.R. Hybrid Multi-Cell Single-Stage Reduced Switch Multilevel Inverter. In Proceedings of the 2020 IEEE International Conference on Power Electronics, Smart Grid and Renewable Energy (PESGRE2020), Cochin, India, 2–4 January 2020; pp. 1–5.